

Coherent error induced phase transition

Hanchen Liu* and Xiao Chen†

Department of Physics, Boston College, Chestnut Hill, Massachusetts 02467, USA

(Dated: June 7, 2025)

We investigate the stability of logical information in quantum stabilizer codes subject to coherent unitary errors. Beginning with a logical state, we apply a random unitary error channel and subsequently measure stabilizer checks, resulting in a syndrome-dependent post-measurement state. By examining both this *syndrome state* and the associated syndrome distribution, we identify a phase transition in the behavior of the logical state. Below a critical error threshold p_c , the syndrome state remains in the same logical state, enabling successful recovery of the code's logical information via suitable error-correction protocols. Above p_c , however, the syndrome state shifts to a different logical state, signaling the breakdown of efficient error correction. Notably, this process can often induce an effective unitary rotation within the logical space. This transition is accompanied by qualitative changes in both the global and local features of the syndrome distribution. We refer to this phenomenon as a *coherent error induced phase transition*. To illustrate this transition, we present two classes of quantum error-correcting code models—the toric code and non-local random stabilizer codes—thereby shedding light on the design and performance limits of quantum error correction under coherent errors.

I. INTRODUCTION

Quantum error-correcting codes (QECCs) are fundamental to achieving fault-tolerant quantum computation, particularly as we progress from the Noisy Intermediate-Scale Quantum (NISQ) era toward fully fault-tolerant quantum computing (FTQC) [1–3]. Preserving quantum information against noise and decoherence is essential for scalable and reliable quantum technologies. Over the past few decades, numerous QECCs have been developed, including topological codes such as the surface code [4–6] and random codes like qLDPC codes [7, 8] and random Clifford codes [9–12]. These codes differ in their resource requirements, threshold error rates, and practical implementation prospects.

A central focus in the field is the characterization of *error thresholds*—the critical error probabilities or strengths at which a QECC transitions from effectively correcting errors to failing catastrophically [3, 4, 13]. These thresholds resemble phase transitions in statistical mechanics [6, 14], offering a framework to benchmark existing error-correction protocols and guide the design of new codes and decoding algorithms.

Early work largely addressed incoherent noise models (e.g., random Pauli channels) [2, 6, 15], which, despite their simplified nature, have yielded deep insights. In particular, they demonstrate the existence of finite thresholds for many codes in the thermodynamic limit [3, 6, 11–13, 16]. More recently, however, there has been increasing interest in the role of *coherent* unitary errors [17–25], rendering them more resistant to standard randomization-based mitigation.

Correcting coherent errors poses added challenges, often necessitating the evaluation of complex-weighted

partition functions analogous to those found in spin glass theory or measurement induced phase transitions [17, 20, 24–34]. Existing studies suggest that the computational difficulty of correcting coherent errors may be linked to underlying phase transitions in both algorithmic and complexity-theoretic contexts [20, 24, 25]. Consequently, examining coherent errors in stabilizer codes can illuminate deep connections among quantum error correction, statistical mechanics, and computational complexity theory.

In this work, we explore a distinct perspective on this topic: the emergence of phase transition in QECCs induced by coherent unitary errors. Specifically, we investigate the stability of logical qubits initially encoded in logical states within quantum stabilizer codes. After coherent unitary errors are applied and syndrome stabilizer measurements are performed, we examine when the encoded logical information remains intact or becomes irreversibly altered or lost.

Our results show that, beyond a certain error threshold p_c , the syndrome measurements can map the original logical stabilizer onto a different one, effectively corrupting the logical information despite the application of error-correction procedures. By computing the coherent information of the associated quantum channel, we identify two distinct modes of error-correction failure. First, the logical information may be partially or entirely lost, resembling the behavior observed under decoherence. Second, the logical information is preserved but transformed—specifically, the coherent error followed by syndrome measurement can induce an effective unitary rotation within the logical space. Below p_c , however, the logical state remains in the same eigenstate (up to a Pauli flip) following the syndrome measurement, enabling successful recovery of the encoded information via appropriate Pauli operations. This transition coincides with a change in the structure of the syndrome distribution function, marking the onset of the *coherent error*

* hanchen.liu@bc.edu

† chenaad@bc.edu

induced phase transition.

To illustrate these findings, we focus on two representative classes of QECC models: the toric code, a canonical example of a topological code [4, 6], and the random stabilizer code ensemble, notable for its potential scaling properties [7–12]. Through numerical simulations, we provide evidence for a critical error density p_c , which separates the recovery and irrecoverable regimes of logical information.

The remainder of this paper is organized as follows. In Sec. II, we review the fundamentals of quantum error-correcting codes and present the coherent error model considered in this work. Sec. II A defines and motivates the notion of quantum error correction and the quantum coherent error. In Sec. III, we apply our methods to the toric code and demonstrate numerical evidence for the coherent error induced phase transition. In Sec. IV, we investigate the coherent error induced phase transition in two representative examples of the random stabilizer code ensemble, namely qLDPC codes and random Clifford codes. Finally, Sec. V summarizes our conclusions and outlines potential avenues for future research.

II. PRELIMINARIES

We begin by reviewing the fundamental concepts of quantum error-correcting codes (QECCs), with a focus on quantum stabilizer codes [2, 15]. A stabilizer code on n qubits is defined by n commuting and independent Pauli operators. These operators generate a group G , known as the stabilizer group. A stabilizer state $|\Psi\rangle$ is a simultaneous eigenstate of all these n commuting Pauli operators.

A $[[n, k, d]]$ quantum stabilizer code encodes k logical qubits into n physical qubits, and is characterized by its code distance d . The code space

$$\mathcal{C} = \{|c\rangle\} \quad (1)$$

is defined as the simultaneous $+1$ eigenspace of $n - k$ independent stabilizer generators (referred to as check operators), which are commuting Pauli string operators and are denoted by $\{h_{i=1,\dots,n-k}\}$. The operators that commute with all check operators form the logical group G_L , and by definition, the code distance d is the minimal weight of all logical operators in G_L :

$$d = \min_{g_L \in G_L} \text{wt}(g_L). \quad (2)$$

When the code state is subjected to a noise channel \mathcal{E} , the encoded state transforms as:

$$\rho_E = \mathcal{E}(|c\rangle\langle c|). \quad (3)$$

To recover the original codeword $|c\rangle$ from the error-affected state ρ_E , we measure the check operators h_i , obtaining measurement outcomes $s_i = \pm 1$. The set $\{s_i\}$,

known as the syndrome, indicates which stabilizer constraints are satisfied or violated. These syndrome values guide the recovery operation needed to restore the encoded quantum information.

A. Coherent error induced phase transition in quantum codes

In this work, we consider quantum codes \mathcal{C} subjected to coherent unitary errors described by the channel

$$\mathcal{E}[\cdot] = \mathcal{U}(\cdot)\mathcal{U}^\dagger, \quad (4)$$

where \mathcal{U} is a unitary operation. We begin with the common eigenstate $|c\rangle$ of the set of k independent commuting logical operators $\{g_{i=1\dots k}\}$, where c is a k -bit binary string specified by the eigenvalue relations:

$$g_i |c\rangle = \lambda_i^c |c\rangle \quad \text{for } i = 1, \dots, k, \quad (5)$$

with $\lambda_i^c = (-1)^{c_i}$ and $c_i \in \{0, 1\}$ denoting the i -th entry of c , corresponding to the eigenvalue of $g_i \in \mathcal{G}_L$. The set of commuting operators $\{g_i\}$ generates the logical stabilizer group

$$\mathcal{G}_L = \langle g_1, \dots, g_k \rangle. \quad (6)$$

The logical stabilizer group \mathcal{G}_L , along with its corresponding set of eigenvalues $\{\lambda_i^c\}$, uniquely determines the code state $|c\rangle$. For convenience, we consider the logical stabilizer group to be a subgroup of the N -qubit Pauli group modulo the Z_2 phase, i.e.,

$$\mathcal{G}_L \subset \mathcal{P}_N / \{\pm 1\}. \quad (7)$$

Next, we introduce an error described by the unitary \mathcal{U} . Acting on the code state $|c\rangle$, it produces the errored state:

$$\rho_E = \mathcal{U}|c\rangle\langle c|\mathcal{U}^\dagger. \quad (8)$$

The specific form of \mathcal{U} depends on the underlying error model, which will be detailed in later sections for each code model.

A standard quantum error correction (QEC) protocol proceeds by measuring the stabilizer checks $\{h_i\}$ after the error occurs. The measurement outcomes form the syndrome $s = \{s_i = \pm 1\}$, and the post-measurement state conditioned on s is given by

$$\rho_s = \mathbb{P}[s]^{-1} \Pi_s \rho_E \Pi_s \quad \text{with} \quad \mathbb{P}[s] = \text{Tr}(\Pi_s \rho_E), \quad (9)$$

where the syndrome projection operator Π_s is defined as

$$\Pi_s = \frac{1}{2^{n-k}} \prod_{i=1}^{n-k} (1 + s_i h_i). \quad (10)$$

We refer to ρ_s as the *syndrome state*. After obtaining the syndrome s , a corresponding unitary U_s is applied to

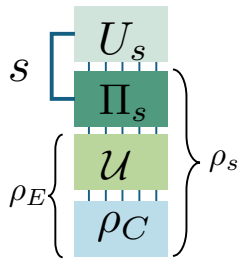


FIG. 1. Quantum error correction (QEC) procedure. To correct the coherent unitary error \mathcal{U} , we first perform the syndrome measurement Π_s to obtain the syndrome s , and then apply the corresponding unitary U_s to correct the error.

correct the error. Figure 1 illustrates this QEC procedure.

Two key elements arise in this framework: the syndrome state ρ_s and the syndrome distribution function $\mathbb{P}[s]$.

- *Syndrome State ρ_s* : The error correction of coherent error presents a fundamental question:

Does the logical stabilizer group $\mathcal{G}_{\mathcal{L}}$ defined in Eq. 6 deform into a distinct group $\mathcal{G}_{\mathcal{L}}'$ under the error-correction procedure described in Eq. 5?

When the logical stabilizer group is deformed—i.e., $\mathcal{G}_{\mathcal{L}} \neq \mathcal{G}_{\mathcal{L}}'$ —the syndrome-based protocol can no longer recover the code state: the deformation itself entails irretrievable loss of quantum information, rendering the error uncorrectable.

- *Syndrome Distribution Function $\mathbb{P}[s]$* : This function provides a direct way to understand how errors spread through the code. A key question is:

How does the coherent error alter the structure of the syndrome distribution?

Analyzing this structural change is crucial for developing new error-correction strategies that can effectively mitigate coherent errors.

In this work, we demonstrate that for coherent unitary errors $\{\mathcal{U}\}$, there exists an error threshold p_c .

- When the error strength p is above the threshold $p > p_c$: Under the QEC procedure, logical stabilizer group $\mathcal{G}_{\mathcal{L}}$ of the code state $|c\rangle$ undergoes a deformation to a different group $\mathcal{G}_{\mathcal{L}}'$. Concurrently, the syndrome distribution $\mathbb{P}[s]$ shifts from exhibiting short-range correlations to long-range correlations. This signifies a loss of logical information due to the error-correction process, rendering the encoded information irrecoverable.
- When the error strength p is below the threshold $p < p_c$: The logical stabilizer group $\mathcal{G}_{\mathcal{L}}$ remains

unchanged, and the syndrome distribution $\mathbb{P}[s]$ retains short-range correlations. This preservation indicates that quantum errors can still be successfully corrected, thus maintaining the integrity of the logical information.

We consider several stabilizer codes and show that in the thermodynamic limit, this threshold corresponds to phase transition, which we refer to as the *coherent error induced phase transition*. This transition closely resembles the measurement-induced transitions explored in previous studies [26–30]. In our models, multi-qubit syndrome measurements can generate nontrivial entanglement within the syndrome state, leading to nonlocal changes in both the logical operators and syndrome distributions. To illustrate these ideas, we study two representative quantum error-correcting code models: the toric code (Sec. III) and random stabilizer codes (specifically, the HGP code, Sec. IV B, and the random Clifford code, Sec. IV C). Through numerical simulations of various quantities, we demonstrate the existence of a critical error threshold p_c that separates the regimes of recoverable and irrecoverable logical information and show that this corresponds to a phase transition in the thermodynamic limit.

III. TORIC CODE

The toric code [4, 6] is defined as the ground state space of the Hamiltonian

$$H = - \sum_v A_v - \sum_p B_p, \quad (11)$$

with the vertex and plaquette operators given by

$$A_v = \prod_{e \in v} X_e, \quad B_p = \prod_{e \in p} Z_e. \quad (12)$$

Here, qubits reside on the edges of a two-dimensional lattice. The operators A_v and B_p apply Pauli- X and Pauli- Z to the edges at vertex v and around plaquette p , respectively as shown in Fig. 2; moreover, $[A_v, B_p] = 0$ for all v and p , so they form a commuting stabilizer check group that defines the code.

As presented on Fig. 2, on a torus, the toric code supports logical operators generated by non-contractable Pauli string operators:

$$Z_{\perp} = \prod_{e \in \perp} Z_e, \quad Z_{\parallel} = \prod_{e \in \parallel} Z_e, \quad (13)$$

$$X_{\perp'} = \prod_{e \in \perp'} X_e, \quad X_{\parallel'} = \prod_{e \in \parallel'} X_e. \quad (14)$$

These non-contractable Pauli string operators commute with all the stabilizer generators but act nontrivially on the code space, resulting in a four-fold degenerate ground state that encodes the quantum information. It

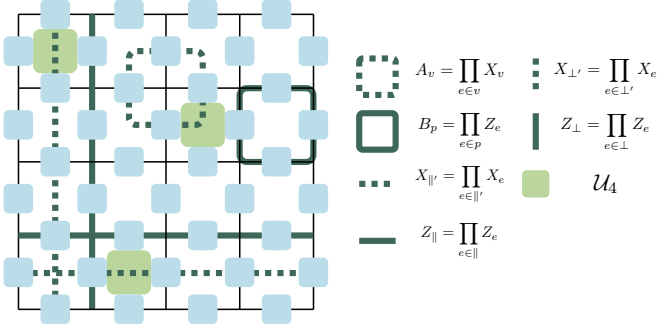


FIG. 2. An illustration of toric code stabilizer checks, logical operators, and the coherent error model. Here, the top and bottom edges, as well as the left and right edges, are identified to form a torus. Qubits reside on the lattice edges. The vertex operator A_v is denoted by a dashed square, while the plaquette operator B_p is denoted by a solid square. The logical operators X_{\perp} and Z_{\perp} appear as vertical thick dashed and solid lines, respectively, while X_{\parallel} and Z_{\parallel} appear as horizontal thick dashed and solid lines. The green plaquettes indicate a random realization of the coherent error unitaries, which are 4-qubit Clifford random unitaries applied with probability p .

is now obvious that the toric code on a $L \times L$ torus is a $[[2L^2, 2, L]]$ quantum code.

For simplicity, we define the logical- Z operators as

$$\bar{Z}_1 = Z_{\perp}, \quad \bar{Z}_2 = X_{\perp}, \quad (15)$$

with both corresponding to the vertical strings shown in Fig. 2. In the following, we begin with the code state

$$|c\rangle = |0_1 0_2\rangle \quad (16)$$

which is the $+1$ eigenstate of \bar{Z}_1 and \bar{Z}_2 . The corresponding logical stabilizer group is thus given by

$$\mathcal{G}_{\mathcal{L}} = \langle \bar{Z}_1, \bar{Z}_2 \rangle. \quad (17)$$

Our error model for the toric code is constructed by applying random 4-qubit Clifford unitaries, \mathcal{U}_4 , which are independently and uniformly sampled from the 4-qubit Clifford unitary group [35]. Each unitary acts on the four qubits of a single plaquette and is applied with probability p , which serves as the error strength parameter. This setup is illustrated in Fig. 2.

A. The Syndrome State

The entanglement properties of the syndrome state ρ_s lie at the heart of understanding the underlying physics of quantum error correction. By examining both local and global aspects, we can uncover how coherent errors and syndrome measurements reshape quantum correlations. Globally, changes in the structure of logical operators and in the coherent quantum information reflect the emergence or dissolution of robust, system-wide error-correcting capabilities [36–38]. Locally, the quantum

conditional mutual information (qCMI) of appropriately chosen subregions reveals the reversibility of quantum information and thus the feasibility of local error-correcting protocols [39]. Taken together, these perspectives on ρ_s offer valuable insights into the principles and effectiveness of quantum error correction.

Syndrome State Logicals

We begin by examining how the logical stabilizer group changes under the error correction procedure. These changes are characterized by the *combined logical group*:

$$G_{\text{comb.}} = \langle \mathcal{G}_{\mathcal{L}}, \mathcal{G}_{\mathcal{L}}', A_v, B_p \rangle / \langle A_v, B_p \rangle, \quad (18)$$

where $\mathcal{G}_{\mathcal{L}}$ is the original logical stabilizer group defined in Eq. 17, $\mathcal{G}_{\mathcal{L}}'$ is the logical stabilizer group of the syndrome state ρ_s , and the quotient by $\langle A_v, B_p \rangle$ removes local redundancies associated with the code check stabilizers.

To quantify how the logical structure evolves, we define the *group difference signature* to be:

$$\Delta_{\text{Logi.}}^{\mathcal{G}'_{\mathcal{L}}} = \log_2 |G_{\text{comb.}}| - \log_2 |\mathcal{G}_{\mathcal{L}}|. \quad (19)$$

If $\Delta_{\text{Logi.}}^{\mathcal{G}'_{\mathcal{L}}} = 0$, the logical stabilizer group is unchanged, indicating that the logical information is potentially preserved. A non-zero $\Delta_{\text{Logi.}}^{\mathcal{G}'_{\mathcal{L}}}$ signals a change in the logical stabilizer group structure, implying a potential loss of logical information.

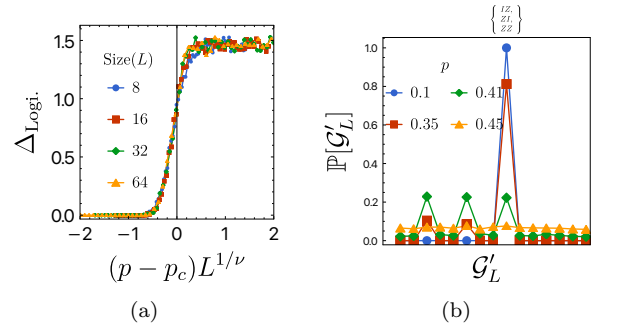


FIG. 3. (a) Change in the number of logical operators, $\Delta_{\text{Logi.}}$, as a function of the error probability p for different system sizes $L = 8, 16, 32, 64$. (b) The syndrome state ρ_s logical stabilizer group \mathcal{G}'_L distribution over 1024 random samples with system size $L = 64$.

As shown in Fig. 3a, we observe a phase transition at $p_c \approx 0.41$:

$$\Delta_{\text{Logi.}}^{\mathcal{G}'_{\mathcal{L}}} = \begin{cases} 0 & p < p_c, \\ 1.46 & p > p_c. \end{cases} \quad (20)$$

Furthermore, the data collapse onto a universal scaling function:

$$\Delta_{\text{Logi.}}^{\mathcal{G}'_{\mathcal{L}}} = f\left(L^{1/\nu}(p - p_c)\right), \quad (21)$$

with a critical exponent $\nu \approx 2.34$. The physical meaning of this exponent will become clear in later sections.

This transition in the *group difference signature* can be understood by examining the change in the logical stabilizer group, $\mathcal{G}_{\mathcal{L}}'$, of the syndrome state ρ_s , with probability distribution $\mathbb{P}[\mathcal{G}_{\mathcal{L}}']$ (see Fig. 3b). For error rates below threshold ($p < p_c$), the distribution is sharply peaked at

$$\mathcal{G}_{\mathcal{L}}' = \mathcal{G}_{\mathcal{L}},$$

where the two groups (up to the sign structure as in Eq. 7) are identical:

$$\mathbb{P}[\mathcal{G}_{\mathcal{L}}'] \sim \delta(\mathcal{G}_{\mathcal{L}}', \mathcal{G}_{\mathcal{L}}).$$

Above threshold ($p > p_c$), the distribution broadens and is effectively uniform:

$$\mathbb{P}[\mathcal{G}_{\mathcal{L}}'] \sim \frac{1}{|\{\mathcal{G}_{\mathcal{L}}'\}|}, \quad (22)$$

where $|\{\mathcal{G}_{\mathcal{L}}'\}|$ is the number of distinct logical stabilizer groups. For a two-logical-qubit code, direct counting yields

$$|\{\mathcal{G}_{\mathcal{L}}'\}| = 3 \times 3 + 6 = 15.$$

Here, the 3×3 groups of the form $\langle O_1 I_2, I_1 O_2 \rangle$ (with $O = X, Y, Z$) are the product state types, and the remaining 6 groups, generated by $\langle O_1 O_2, O'_1 O'_2 \rangle$, are the Bell pair types.

The distribution of the *group difference signature*, $\Delta_{\text{Logi.}}^{\mathcal{G}_{\mathcal{L}}'}$, is given in Table I. Its expectation value,

$$\overline{\Delta_{\text{Logi.}}} = \sum_{\mathcal{G}_{\mathcal{L}}'} \mathbb{P}[\mathcal{G}_{\mathcal{L}}'] \Delta_{\text{Logi.}}^{\mathcal{G}_{\mathcal{L}}'} = \frac{22}{15} \approx 1.46,$$

matches the numerical simulation.

$\Delta_{\text{Logi.}}^{\mathcal{G}_{\mathcal{L}}'}$	$\langle O_1, O_2 \rangle$	$\langle O_1 O_2, O'_1 O'_2 \rangle$
0	1/15	0
1	4/15	2/15
2	4/15	4/15

TABLE I. Probability distribution of $\Delta_{\text{Logi.}}^{\mathcal{G}_{\mathcal{L}}'}$, $\mathcal{G}_{\mathcal{L}}' = 0, 1, 2$ for different types of logical stabilizer groups: product state type $\langle O_1, O_2 \rangle$ and Bell pair type $\langle O_1 O_2, O'_1 O'_2 \rangle$.

This result indicates a critical phase transition in the logical stabilizer structure of the toric code. Below p_c , the logical stabilizer group remains unchanged, ensuring that the logical information is fully preserved. Above p_c , however, the structure of the logical stabilizer group is altered in a random manner, signaling a loss of logical information. Thus, p_c serves as a coherent error threshold, a point beyond which the logical information can no longer be reliably maintained. This conclusion is further supported by the analyses presented in the following sections.

B. Effective quantum channel

The coherent error phase transition can also be treated via the quantum channel language from the quantum information theoretical perspective.

For a coherent unitary error, the error channel is obtained as follows. For a typical QEC protocol—as illustrated in Fig. 1—the overall quantum channel is

$$\begin{aligned} \mathcal{E}_{re}(\cdot) &= \sum_s U_s \Pi_s \mathcal{U}(\cdot) U_s^\dagger \Pi_s U_s^\dagger \\ &= \sum_s U_s \Pi_s \left(\sum_{s'} \Pi_{s'} \mathcal{U}(\cdot) U_s^\dagger \Pi_{s'} \right) \Pi_s U_s^\dagger \\ &= \mathcal{E}_r \circ \mathcal{E}_e(\cdot), \end{aligned} \quad (23)$$

where U_s is the error-correction unitary corresponding to syndrome s , Π_s is the syndrome projector, and \mathcal{U} denotes the coherent unitary error. The channel \mathcal{E}_{re} now decomposes as:

- *Error correction channel:*

$$\mathcal{E}_r(\cdot) = \sum_s U_s \Pi_s (\cdot) \Pi_s U_s^\dagger, \quad (24)$$

- *Effective coherent noise channel:*

$$\mathcal{E}_e(\cdot) = \sum_s \Pi_s \mathcal{U}(\cdot) U_s^\dagger \Pi_s. \quad (25)$$

The effective noise channel can also be expressed as an average over syndrome outcomes:

$$\overline{\rho_s} = \sum_s \mathbb{P}[s] \rho_s = \sum_s \Pi_s \rho_E \Pi_s, \quad (26)$$

where ρ_E and ρ_s are the errored state and syndrome state defined in Eqs. 8 and 9, respectively.

In what follows, we focus on two key aspects of the effective quantum channel \mathcal{E}_e : the local structure of the resulting error-affected state $\overline{\rho_s}$, as measured by the quantum conditional mutual information (qCMI), and the global performance of \mathcal{E}_e , as measured by the quantum coherent information (qCI), which directly quantifies the channel's quantum information loss.

Quantum conditional mutual information and local entanglement structure

We investigate the quantum conditional mutual information (qCMI) of the quantum state

$$\overline{\rho_s} = \mathcal{E}_e(\rho_0). \quad (27)$$

Here, we take the code state to be a pure state $\rho_0 = |0_1, 0_2\rangle \langle 0_1, 0_2|$, i.e. the eigenstate of the logical operators \overline{Z}_1 and \overline{Z}_2 defined in Eq. 16, and the noise channel \mathcal{E}_e is defined in Eq. 25.

For three regions A , B , and C , the qCMI is defined as

$$I(AB | C)_{\bar{\rho}_s} = [S(\bar{\rho}_s^{AC}) - S(\bar{\rho}_s^C)] - [S(\bar{\rho}_s^{ABC}) - S(\bar{\rho}_s^{BC})], \quad (28)$$

where for any domain $\mathcal{D} \in \{AC, BC, C, ABC\}$, the von Neumann entropy is given by

$$S(\bar{\rho}_s^{\mathcal{D}}) = -\text{Tr}(\bar{\rho}_s^{\mathcal{D}} \log \bar{\rho}_s^{\mathcal{D}}), \quad (29)$$

with $\bar{\rho}_s^{\mathcal{D}} = \text{Tr}_{\bar{\mathcal{D}}} \bar{\rho}_s$.

In our setup, the noisy toric code state $\rho_{Q'}$ is defined on a torus, with regions A and B being non-overlapping rings and region $C = \overline{AB}$ its complement (see Fig. 4a).

In contrast to the global recoverability transition captured by the coherent information in the previous section, the qCMI characterizes local structure of the phase transition in two key ways:

a. Local Recoverability and Mixed State Phases: The qCMI quantifies whether local recovery channels are sufficient for error correction. In particular, for two distant regions A and B , the qCMI scales as $I(AB | C)_{\bar{\rho}_s} \sim O(\exp(-d_{AB}/\xi))$, with the length scale ξ captures the size of the recovery channel needed, and the divergence of ξ indicates the phase transition of the mixed state [39–43].

b. Entanglement Structure: The qCMI also reflects changes in the entanglement structure of the errored state. For stabilizer systems, $I(AB | C)_{\bar{\rho}_s}$ effectively counts the number of stabilizers connecting regions A and B . This can be formalized via the group quotient

$$I(AB | C)_{\bar{\rho}_s} = \log \left| \frac{G^C}{G_A^C \cdot G_B^C} \right|, \quad (30)$$

where $G^C \equiv G/G_C$ with $G_C \subset G$ being the subgroup whose elements are supported only in C , and $G_A^C \equiv G_{AC}/G_C$ and $G_B^C \equiv G_{BC}/G_C$ where G_{AB}, G_{AC}, G_C are the subgroups localized in regions AC , BC , and C , respectively. Intuitively, this quotient counts the number of nontrivial Pauli operators shared by A and B , thereby capturing the size of the stabilizer operators connecting these regions. Such an algebraic structure has been studied previously in the context of random plaquette models [44].

As shown in Fig. 4, the qCMI is zero when $p < p_c$ and is finite when $p > p_c$. At the critical point $p = p_c$, the qCMI exhibits a power-law decay:

$$I(AB | C)_{\bar{\rho}_s} \sim u^{-\alpha}, \quad \text{with } \alpha = 0.5, \quad (31)$$

where $u = \sin(\pi d_{AB}/L)$ and d_{AB} is the separation between regions A and B . Fixing $d_{AB} = L/2$, the qCMI data collapses onto a universal scaling form:

$$I(AB | C)_{\bar{\rho}_s} \sim f(L^{1/\nu}(p - p_c)), \quad (32)$$

with a critical error probability $p_c = 0.41$ and a critical exponent $\nu = 2.34$ (consistent with results in Eq. 21 and

Eq. 47). This scaling implies that the length scale of the stabilizer operators in the errored state diverges near p_c :

$$\xi \sim \frac{1}{(p - p_c)^\nu}. \quad (33)$$

Thus, above the critical probability ($p > p_c$), stabilizers induced by syndrome measurements become arbitrarily large, directly influencing the global logical structure discussed earlier.

In the sections that follow, we will show that this quantum stabilizer behavior is also reflected in the classical information encoded in the syndrome distribution $\mathbb{P}[s]$. Together, these results provide strong evidence that a true phase transition governs the error-correction capabilities of the toric code under coherent errors.

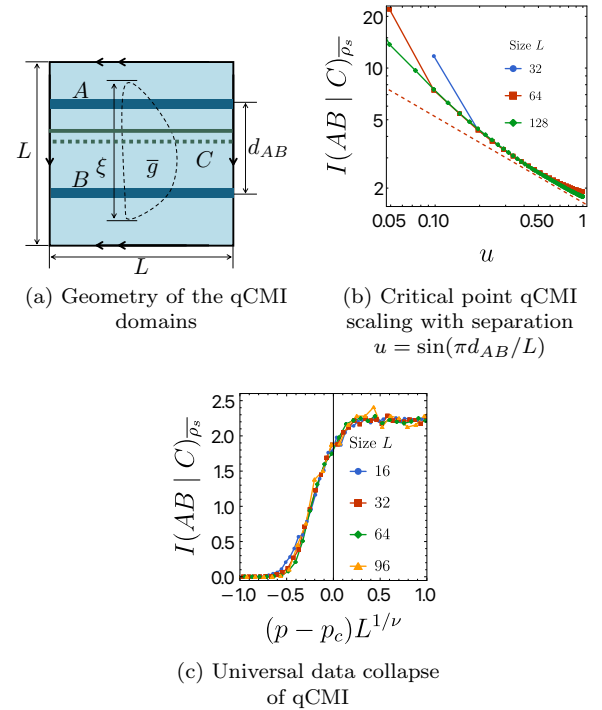


FIG. 4. (a) Geometry of the regions A , B , and C used to define the qCMI. Dark blue strips denote regions A and B , while the light blue area indicates C . A non-local stabilizer \bar{g} (dashed lines) has a characteristic length scale ξ . The solid dashed lines, parallel to A and B , represent the two logical stabilizers of the toric code state ρ_0 . Identical arrows on the boundaries indicate periodic boundary conditions. (b) Numerical data showing qCMI decay at $p = 0.41$: $I(AB | C)_{\bar{\rho}_s} \sim u^{-0.5}$, where $u = \sin(\pi d_{AB}/L)$. (c) Universal data collapse of $I(AB | C)_{\bar{\rho}_s}$ as a function of $L^{1/\nu}(p - p_c)$ with $\nu = 2.34$ near the critical point.

Coherent Information

To confirm that the transition in the logical stabilizer structure corresponds to an error-correction phase tran-

sition, we compute the *quantum coherent information* (qCI) of the noise error channel \mathcal{E}_e , which is defined as the difference between two entropies, i.e.,

$$I(\rho_Q, \mathcal{E}_e) = S(\rho_{Q'}) - S(\rho_{RQ'}), \quad (34)$$

where $\rho_{Q'}$ is the output state after applying the channel \mathcal{E}_e to the initial quantum code state ρ_Q

$$\rho_{Q'} = \mathcal{E}_e(\rho_Q), \quad (35)$$

and $\rho_{RQ'}$ is the output of the joint state of the reference system R and the original quantum code Q after the extended quantum channel

$$\rho_{RQ'} = (\mathcal{I}_R \otimes \mathcal{E}_e)(\rho_{RQ}). \quad (36)$$

Here, \mathcal{I}_R is the identity on R and

$$\rho_{RQ} = |\Psi_{RQ}\rangle \langle \Psi_{RQ}| \quad (37)$$

is a purification of the quantum code state ρ_Q (with $\rho_Q = \text{Tr}_R \rho_{RQ}$). The qCI quantifies the amount of recoverable quantum information of the noise channel \mathcal{E}_e . In fact, by treating the QEC protocol as a composite quantum channel as present in Eq. 23

$$\mathcal{E}_{re} = \mathcal{E}_r \circ \mathcal{E}_e, \quad (38)$$

where \mathcal{E}_e is the error channel and \mathcal{E}_r implements error correction. It has been shown that perfect quantum error correction exists if and only if

$$I(\rho_Q, \mathcal{E}_e) = S(\rho_Q), \quad (39)$$

i.e. when the qCI of the error channel equals the entropy of the quantum code [36–38].

Now, we choose the code state ρ_Q as the maximally mixed state in the code space \mathcal{C} :

$$\rho_Q = \frac{1}{2^k} \sum_c |c\rangle \langle c|, \quad (40)$$

with the summation over all k -bit binary strings c corresponding to the logical stabilizer group $\mathcal{G}_L = \langle g_1, \dots, g_k \rangle$ (see Eq. 5). It follows that

$$S(\rho_Q) = k. \quad (41)$$

Throughout, all logarithms are base 2.

A natural purification is obtained by introducing k reference qubits, each maximally entangled with one of the k logical qubits via Bell states:

$$|\text{Bell}_i\rangle = \frac{1}{\sqrt{2}} \left(|0\rangle_i \otimes |0\rangle_i^r + |1\rangle_i \otimes |1\rangle_i^r \right), \quad i = 1, \dots, k. \quad (42)$$

Here, $|0\rangle_i$ and $|1\rangle_i$ are the eigenstates of the generator $g_i \in \mathcal{G}_L$, and $|0\rangle_i^r, |1\rangle_i^r$ are the Pauli- Z eigenstates (with eigenvalues ± 1) of the i th reference qubit. The purified state is then

$$\rho_{RQ} = |\Psi_{RQ}\rangle \langle \Psi_{RQ}|, \quad \text{with } |\Psi_{RQ}\rangle = \bigotimes_{i=1}^k |\text{Bell}_i\rangle. \quad (43)$$

After sending this purified state through the extended noise channel,

$$\rho_{RQ'} = (\mathcal{I}_R \otimes \mathcal{E}_e)(\rho_{RQ}), \quad (44)$$

perfect quantum error correction can be achieved when the qCI of \mathcal{E}_e satisfies

$$I(\rho_Q, \mathcal{E}_e) = S(\rho_{Q'}) - S(\rho_{RQ'}) = k, \quad (45)$$

where $\rho_{Q'} = \mathcal{E}_e(\rho_Q)$.

In the case of a toric code defined on a torus, we have $k = 2$. As illustrated in Fig. 5, the coherent information $I(\rho_Q, \mathcal{E}_e)$ for the coherent noise channel \mathcal{E}_e exhibits the following behavior:

$$I(\rho_Q, \mathcal{E}_e) = \begin{cases} 2, & p < p_c, \\ 1.2, & p > p_c, \end{cases} \quad (46)$$

with a critical error probability $p_c \approx 0.41$. Moreover, the data collapse onto a universal scaling function,

$$I(\rho_Q, \mathcal{E}_e) = g(L^{1/\nu}(p - p_c)), \quad (47)$$

with the critical exponent $\nu \approx 2.43$. When $p < p_c$ we have $I(\rho_Q, \mathcal{E}_e) = 2$, indicating that a global error correction protocol can fully correct the coherent error; for $p > p_c$, the averaged $I(\rho_Q, \mathcal{E}_e) \approx 1.2 < 2$. We further apply a deep random unitary circuit to generate a random stabilizer state, followed by syndrome measurement, and observe a similar value of $I \approx 1.2$ in this setup. The successful data collapse around p_c strongly indicates the presence of a phase transition.

Since we are working with stabilizer states, the coherent information for each realization of coherent error can only take discrete values: 2, 1, or 0. When the coherent information $I(\rho_Q, \mathcal{E}_e) = 2$, the logical information is fully preserved, and thus the coherent error followed by syndrome measurement induces an effective *unitary operation* on the logical qubits, altering the encoded information without destroying it. For the syndrome state described in Eq. 5, this operation effectively corresponds to a unitary evolution of the logical stabilizer state. As the logical state has changed, the original information cannot be recovered. $I(\rho_Q, \mathcal{E}_e) = 1$ or $I(\rho_Q, \mathcal{E}_e) = 0$ indicates a partial or complete loss of quantum information. For syndrome states characterized by initially distinct logical groups, these states may become indistinguishable after the error, meaning the error has degraded or entirely destroyed the logical information.

This confirms that the observed transition in the logical stabilizer structure corresponds to an error-correction phase transition, with p_c marking the threshold that separates the recoverable phase from one in which logical information cannot be reliably restored.

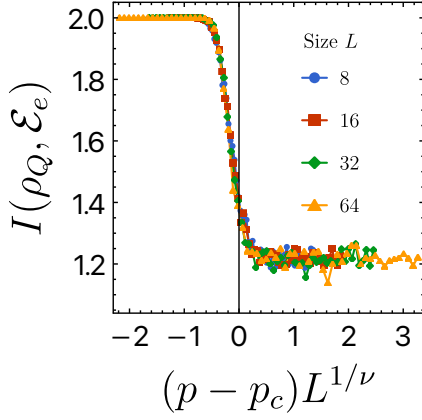


FIG. 5. Coherent information $I(\rho_Q, \mathcal{E}_e)$ as a function of the error probability p for different system sizes $L = 8, 16, 32, 64$.

C. Syndrome Distribution

We now turn our attention to the syndrome distribution function,

$$\mathbb{P}[s] = \text{Tr}(\Pi_s \rho_E), \quad (48)$$

which gives the probability of obtaining a particular syndrome s .

Here, we take the error state ρ_E stabilizer group to be

$$G_E = \langle \tilde{g}_1, \dots, \tilde{g}_N \rangle, \quad (49)$$

where the \tilde{g}_i 's are Pauli strings with charges $\lambda_i = \pm 1$ satisfying

$$\tilde{g}_i \rho_E = \lambda_i \rho_E. \quad (50)$$

The syndrome distribution can be expressed explicitly as (see App. A for details)

$$\mathbb{P}[s] = Z^{-1} \prod_{k=1}^{r_Q} \delta_k[s], \quad (51)$$

where

$$\delta_k[s] = \frac{1}{2} \left(1 + q_k \lambda_k \prod_{i=1}^{N_s} (s_i)^{Q_{i,k}} \right). \quad (52)$$

Here, $\lambda_k = \pm 1$ denotes the charge associated with the k -th stabilizer in Eq. 49, $q_k = \pm 1$ is the sign structure of the check observables, and $Q_{i,k} \in \{0, 1\}$ is the incidence matrix specifying the support of the stabilizer on the measurement outcomes. In addition, N_s denotes the total number of measurements, and r_Q is the number of independent constraints that emerge from the quantum Pauli measurement process. The normalization factor Z is the partition function:

$$Z = \sum_s \prod_{k=1}^{r_Q} \delta_k[s] = 2^{N_s - r_Q}. \quad (53)$$

In the following, we study both the global and local structures of the syndrome distribution.

The Classical Conditional Mutual Information

To probe the structure of the syndrome distribution, we consider the classical conditional mutual information (CMI) of two regions A and B , conditioned on a third region C , as illustrated in Fig. 6a:

$$I(AB | C)_{\mathbb{P}} = \sum_s \mathbb{P}[s] \log \frac{\mathbb{P}_C[s_C] \mathbb{P}[s]}{\mathbb{P}_{AC}[s_{AC}] \mathbb{P}_{BC}[s_{BC}]}, \quad (54)$$

where $\mathbb{P}_{\mathcal{D}}[s_{\mathcal{D}}]$ denotes the marginal probability distribution over outcomes restricted to the domain \mathcal{D} .

The CMI measures whether the random variables associated with regions A , C , and B form a Markov chain. In particular, $I(AB | C)_{\mathbb{P}} \geq 0$ with equality if and only if A , C , and B form a Markov chain [45]. When $I(AB | C)_{\mathbb{P}} = 0$, A and B are conditionally independent given C , meaning that no non-local information is shared among the regions.

Conversely, a nonzero CMI indicates that global correlations exist among A , B , and C . In our context, such global structure in the syndrome readout suggests that quantum logical information is being inadvertently revealed, thereby signaling quantum information loss in the syndrome measurement process.

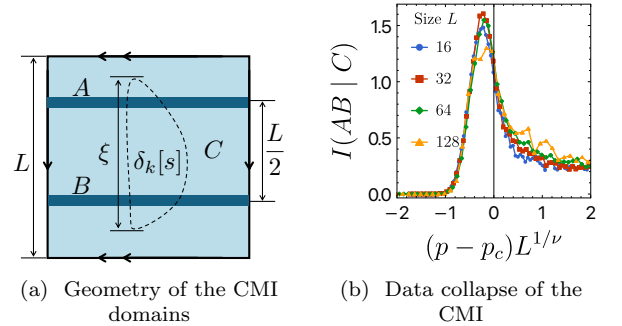


FIG. 6. (a) Geometry of regions A , B , and C . The dark blue strips represent A and B , while the light blue region represents C . A non-local constraint $\delta_k[s]$ is indicated by dashed lines, with a characteristic length scale ξ . Identical arrows on the boundaries indicate periodic boundary conditions. (b) Numerical data collapse of $I(AB | C)$, demonstrating universal scaling near the critical point.

For stabilizer systems, the conditional mutual information (CMI) of the syndrome distribution $\mathbb{P}[s]$ can be calculated as follows.

First, the marginal distribution over outcomes in a domain \mathcal{D} is obtained by summing over the syndromes outside \mathcal{D} :

$$\mathbb{P}_{\mathcal{D}}[s_{\mathcal{D}}] = \sum_{s_{\overline{\mathcal{D}}}} Z^{-1} \prod_{k=1}^{r_Q} \delta_k[s] = Z_{\mathcal{D}}^{-1} \prod_{k=1}^{r_Q} \delta_k^{\mathcal{D}}[s], \quad (55)$$

where

$$\delta_k^{\mathcal{D}}[s] = \frac{1}{2} \left(1 + q_k \lambda_k \prod_{i \in \mathcal{D}} (s_i)^{Q_{i,k}} \right) \quad (56)$$

represents the local constraint on the syndromes, $Q^{\mathcal{D}} \subset Q$ is the restriction of the binary matrix Q to the domain \mathcal{D} , and $r_{Q^{\mathcal{D}}}$ is the number of independent entries in $Q^{\mathcal{D}}$. The dimension of $Q^{\mathcal{D}}$ is given by

$$\dim(Q^{\mathcal{D}}) = r_Q - \text{rank}(Q_{\overline{\mathcal{D}}}), \quad (57)$$

where $Q_{\overline{\mathcal{D}}}$ is the submatrix of Q corresponding to the complement of \mathcal{D} . The local partition function is then

$$Z_{\mathcal{D}} = 2^{|\mathcal{D}| - \dim(Q^{\mathcal{D}})}. \quad (58)$$

We define the *local free entropy* for domain \mathcal{D} as

$$\phi_{\mathcal{D}} \equiv \log_2 Z_{\mathcal{D}} = |\mathcal{D}| - \dim(Q^{\mathcal{D}}), \quad (59)$$

and the *global free entropy* as

$$\phi \equiv \log_2 Z = N_s - r_Q, \quad (60)$$

where N_s is the total number of syndrome bits.

Combining these results, the conditional mutual information takes a simple form:

$$\begin{aligned} I(AB | C) &= \phi_{AC} + \phi_{BC} - \phi_C - \phi \\ &= \text{rank}(Q_A) + \text{rank}(Q_B) - \text{rank}(Q_{AB}), \end{aligned} \quad (61)$$

which shows that the CMI counts the number of independent constraints shared by domains A and B .

For geometry shown in Fig. 6a, we can introduce a length scale ξ for the constraints $\delta_k[s]$. Similar to the quantum scenario near p_c , the typical constraint length scale diverges as:

$$\xi \sim |p - p_c|^{-\nu}, \quad (62)$$

leading to:

$$I(AB | C) = f(L^{1/\nu}(p - p_c)), \quad (63)$$

where L is the system size and f is some scaling function. The data collapse in Fig. 6b confirms universal scaling behavior and matches the critical exponents ($\nu = 2.34$) extracted from the logical operator analysis.

Global Information

Having explored the spatial structure of the syndrome configurations $s = \{s_i = \pm 1\}$, we now consider their global properties. Recall that the syndrome distribution takes the form

$$\mathbb{P}[s] = Z^{-1} \prod_{k=1}^{r_Q} \delta_k[s],$$

with the partition function given by

$$Z = \sum_s \prod_{k=1}^{r_Q} \delta_k[s] = 2^{N_s - r_Q},$$

where r_Q is the number of constraints and N_s is the total number of syndrome degrees of freedom. The Shannon entropy of this distribution is

$$S_{\mathbb{P}} = - \sum_s \mathbb{P}[s] \log \mathbb{P}[s] = \log Z, \quad (64)$$

which coincides with the *free entropy* defined in Eq. 60:

$$\phi = N_s - r_Q. \quad (65)$$

This free entropy reflects the number of constraints $\delta[s]$ that emerge from the quantum measurement process. In the absence of any constraints, the distribution is uniform, yielding $S_{\mathbb{P}} = \phi = N_s$; conversely, if there are N_s constraints, the measurement outcomes $\{s\}$ are fixed to a unique configuration, so that $S_{\mathbb{P}} = \phi = 0$. Thus, the number of emergent constraints directly characterizes the global structure of $\mathbb{P}[s]$.

To directly capture the number of emergent constraints in the measurement process, we define the *reduced free entropy density* as

$$\varphi \equiv 1 - \frac{\phi}{N_s} = \frac{r_Q}{N_s}, \quad (66)$$

where $\phi = \log_2 Z = N_s - r_Q$ is the global free entropy. This quantity φ provides a normalized measure of the number of constraints relative to the total syndrome degrees of freedom.

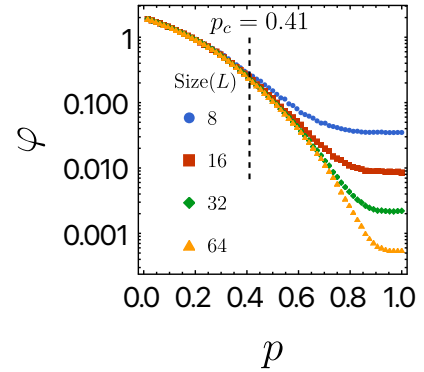


FIG. 7. The scaling of the reduced free entropy density φ , as a function of the error probability p , for different system sizes $L = 8, 16, 32, 64$.

As shown in Fig. 7, for $p < p_c$, the reduced free entropy density $\varphi(p)$ converges, indicating an extensive number of constraints that scale with N . However, for $p > p_c$, the number of constraints does not remain extensive, indicating that the distribution function approaches the uniform distribution as the system size becomes large, and that reflects a fundamental change in the global structure of the syndrome distribution.

In summary, both local and global properties of the syndrome distribution exhibit critical behavior near p_c . Below p_c , an extensive set of constraints enforces a

highly structured syndrome distribution, whereas above p_c , this structure breaks down, consistent with the error-correction phase transition uncovered in the previous analyses. We thus finish analyzing the coherent error induced phase transition in the toric code model.

IV. THE RANDOM STABILIZER CODE ENSEMBLE

In this section, we present two examples of the *random stabilizer code ensemble* (RSCE) that can maintain a constant code rate. This contrasts to topological codes such as the toric code, where the code space remains $O(1)$ and the rate becomes infinitesimal as the size of the system increases.

We begin with a structured example: quantum low-density parity-check (qLDPC) codes derived from the hypergraph product of two classical LDPC codes[46], the HGP codes [7, 8]. These codes inherit robust error-correcting properties from their classical counterparts and support an extensive number of logical qubits.

Next, we consider the simplest scenario: *Random Clifford Codes*(RCC)[9–12], generated by random Clifford circuits. Despite their simplicity, random Clifford codes exhibit intriguing features, including information scrambling properties and a high encoding rate.

In both examples, the quantum codes are random in nature, yet they sustain a code rate that remains finite in the thermodynamic limit. We consider both cases under coherent errors and demonstrate the existence of an error-correction phase transition.

A. Coherent Random q -Unitary Error

In the context of RSCEs, we analyze two types of coherent errors. The first type, the long-ranged q -error, occurs when unitary noise is applied to q qubits that are randomly selected irrespective of their code structure. In contrast, the short-ranged q -error involves the selection of q errored qubits based on the underlying structure of the code.

In the long-range model, each physical qubit i randomly selects $q - 1$ other qubits, and a Clifford q -unitary is applied to this group with probability p . In the extreme case where $p = 1$ and $q = 1$, each qubit independently undergoes a single-qubit Clifford rotation, yielding fully local and uncorrelated errors.

By contrast, the short-ranged q -error confines each multi-qubit unitary to a cluster of q qubits that are neighbors in the underlying code structure. In an HGP code, these q -local interactions occur among qubits connected by edges in the hypergraph product. Concretely, for each qubit i , one selects $q - 1$ adjacent qubits via a random walk of length $q - 1$ on the hypergraph product, then applies a q -qubit Clifford gate with probability p . In a random Clifford code (RCC), similar constraints hold,

but the notion of neighboring qubits derives from the local random gates defining the code.

When $q = 1$, both models coincide, because each error reduces to an independent single-qubit Clifford rotation on every qubit, thus removing any distinction between long-range and local interactions.

B. HGP Code

In this section, we discuss the coherent error phase transition in the hypergraph product (HGP) code[7, 8]. The HGP code, denoted by \mathcal{C} , is a CSS code constructed from two classical linear codes C_1 and C_2 over \mathbb{F}_2 , with parity-check matrices H_1 and H_2 . The qubits of the HGP code reside on the edges of the bipartite graph formed by taking the product of the Tanner graphs associated with C_1 and C_2 .

Code Construction

The stabilizer generators of the HGP code are:

$$\begin{aligned} H_X &= \begin{pmatrix} H_1 \otimes I_{n_2} & I_{r_1} \otimes H_2^\top \end{pmatrix}, \\ H_Z &= \begin{pmatrix} I_{n_1} \otimes H_2 & H_1^\top \otimes I_{r_2} \end{pmatrix}, \end{aligned} \quad (67)$$

where n_i and r_i are the lengths and ranks (numbers of checks) of the codes C_i and C_i^\top , respectively. The total number of physical qubits is

$$N = n_1 n_2 + r_1 r_2. \quad (68)$$

For simplicity, we choose random LDPC codes C_1 and C_2 of length N . The logical X operators of the HGP code correspond to codewords in $C_1^\perp \otimes C_2$ and $C_1 \otimes C_2^\perp$ that are not generated by the check matrices H_X or H_Z . Concretely:

For $v_1 \in \mathbb{F}_2^{n_1} \setminus \text{im}(H_1)$ and $v_2 \in \ker(H_2)$, the tensor product $v_1 \otimes v_2$ defines a logical X operator:

$$X^I = (v_1 \otimes v_2 | 0). \quad (69)$$

For $v'_1 \in \ker(H_1^\top)$ and $v'_2 \in \mathbb{F}_2^{r_2} \setminus \text{im}(H_2^\top)$, the tensor product $v'_1 \otimes v'_2$ defines another logical X :

$$X^{II} = (0 | v'_1 \otimes v'_2). \quad (70)$$

Logical Z operators arise similarly, using codewords in C_1 and H_2^\perp . The total number of logical qubits is

$$K = k_1 k_2 + k_1^\top k_2^\top, \quad (71)$$

and the code distance satisfies

$$D = \min\{d_1, d_2, d_1^\top, d_2^\top\}, \quad (72)$$

where d_1, d_2 (and d_1^\top, d_2^\top) are the distances of C_1, C_2 (and C_1^\top, C_2^\top), respectively.

Example Setup. For instance, let H_1 and H_2 be random LDPC $_n(3, 6)$ codes, where the code contains a total of n -bits, each check contains 6 bits and each bit is shared by 3 checks, and the desired code rate is $1/2$. [47] Then, for the HGP code,

$$N \sim \frac{5}{4} n^2, \quad K \sim \frac{1}{4} n^2 \quad (73)$$

Syndrome Measurement

A coherent error model is introduced by selecting a random Clifford q -unitary on q qubits with probability p as present previously in Sec. IV A. The stabilizers H_X and H_Z are then measured, yielding a syndrome $s = \{s^X, s^Z\}$. The post-measurement state is

$$\rho_s = \mathbb{P}[s]^{-1} \Pi_X^{s^X} \Pi_Z^{s^Z} \rho \Pi_Z^{s^Z} \Pi_X^{s^X}, \quad (74)$$

where

$$\begin{aligned} \Pi_X^{s^X} &= \prod_{i=1}^{r_1 n_2} \frac{1}{2} \left(1 + s_i^X \prod_{j=1}^N X_j^{(H_X)_{i,j}} \right), \\ \Pi_Z^{s^Z} &= \prod_{i=1}^{r_2 n_1} \frac{1}{2} \left(1 + s_i^Z \prod_{j=1}^N Z_j^{(H_Z)_{i,j}} \right), \end{aligned} \quad (75)$$

and $\mathbb{P}[s]$ is the probability of obtaining syndrome s .

Analogously to the toric code, we analyze both the post-measurement state ρ_s (and its stabilizer properties) and the classical syndrome distribution $\mathbb{P}[s]$. We show that a coherent error induced phase transition emerges at some threshold p_c . Below p_c , the logical information encoded by the HGP code remains protected. Above p_c , unlike the toric code (which has finite chance to lose logical information), we will show that the random code in the thermodynamic limit retains its logical space but scrambles it, rendering practical decoding infeasible in finite time.

Syndrome State Logicals

We now investigate how coherent errors modify the logical stabilizer group of the HGP code by examining the *combined logical group* (previously defined in Eq. 18). For HGP codes, this group is given by

$$G_{\text{comb}} = \langle X^I, X^{II}, G'_L, H_X, H_Z \rangle / \langle H_X, H_Z \rangle, \quad (76)$$

where $\langle X^I, X^{II} \rangle$ are the initial logical stabilizers given in Eq. 69 and 70, and G'_L represents the emergent logical operators in the post-measurement syndrome state. The change in logical operators is quantified by the *group difference signature*

$$\Delta_{\text{Logi.}} = \log_2 |G_{\text{comb}}| - \log_2 |\langle X^I, X^{II} \rangle|. \quad (77)$$

Since the HGP code has a finite code rate, we normalize by the total number of logical qubits K :

$$\delta_{\text{Logi.}} = \frac{1}{K} \Delta_{\text{Logi.}}. \quad (78)$$

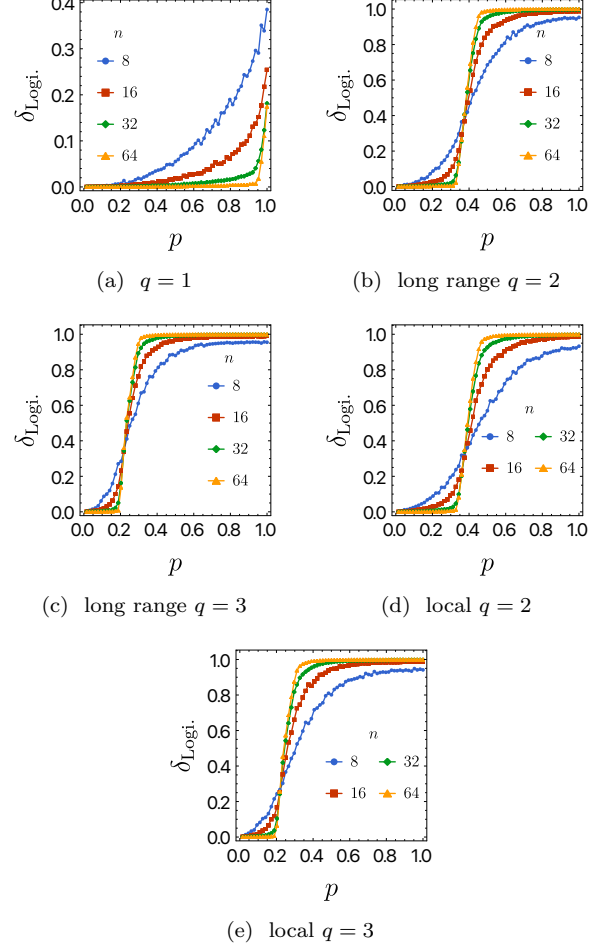


FIG. 8. Change in the density of logical operators, $\delta_{\text{Logi.}}$, versus the error rate p for different code sizes $n = 8, 16, 32, 64$. Plot (a) shows the single site random unitary model, plots (b)–(c) correspond to the long-range q -unitary model with $q = 1, 2, 3$, while (d)–(e) illustrate the q -local model. Each HGP code is constructed from LDPC $_n(3, 6)$ with $n = 8, 16, 32, 64$.

Figure 8 shows that, for an HGP code built from LDPC $_n(3, 6) \times \text{LDPC}_n(3, 6)$, a phase transition appears at a threshold p_c under both the long-range and q -local models. For $q > 1$, we observe:

$$\delta_{\text{Logi.}} = \begin{cases} 0 & p < p_c, \\ 1 & p > p_c, \end{cases} \quad (79)$$

whereas for $q = 1$, we still find a transition between $\delta_{\text{Logi.}} = 0$ for $p < p_c$ and $\delta_{\text{Logi.}} > 0$ for $p > p_c$.

In essence, once the error strength p exceeds p_c , the logical operators undergo a fundamental alteration, signaling that the encoded logical information can no longer

be recovered through a straightforward decoding scheme. In the following, we reinforce this conclusion by examining coherent logical information.

Coherent Logical Information

We quantify the *logical coherent information* of the HGP code by coupling each of its K logical qubits to a corresponding reference qubit, thereby forming K Bell pairs. Concretely, we consider the state

$$|\Psi\rangle = \bigotimes_{i=1}^K |\text{Bell}_i\rangle \quad (80)$$

where

$$|\text{Bell}_i\rangle = \frac{1}{\sqrt{2}} \left(|0\rangle_i \otimes |0\rangle_i^r + |1\rangle_i \otimes |1\rangle_i^r \right), \quad i = 1, \dots, k. \quad (81)$$

are bell pairs given by the i -th logical qubit and i -th reference qubit.

Since the HGP code supports a macroscopic number K of logical qubits, we focus on the *per-logical-qubit* coherent information:

$$\bar{I}_c = \frac{1}{K} I(\rho_Q, \mathcal{E}_e), \quad (82)$$

where $I(\rho_Q, \mathcal{E}_e)$ (see Eq. 34) is the total coherent information and K is the total number of logical qubits with $\rho_Q = |\Psi\rangle\langle\Psi|$. This quantity measures the average quantum information retained under the coherent noise channel as previously shown in Eq. 25,

$$\mathcal{E}_e(\cdot) = \sum_s \Pi_s \mathcal{U}(\cdot) \mathcal{U}^\dagger \Pi_s, \quad (83)$$

where \mathcal{U} represents the unitary error and Π_s denotes the projector corresponding to syndrome s . As presented in previous sections, \bar{I}_c directly quantifies the loss of logical information induced by coherent errors.

As shown in Fig. 9, the *per-logical-qubit* coherent information follows the scaling:

$$\bar{I}_c \approx \exp\left(-\frac{h(p)}{N}\right), \quad (84)$$

where $h(p) \geq 0$ is some function of the error rate p , and N is the total number of physical qubits. Notably, the loss of information is *suppressed* as the system size N grows. This indicates the error channel is effectively unitary when $N \rightarrow \infty$.

Combining this observation with the results from the previous subsection—where the logical stabilizers remain unaltered for $p < p_c$ and fully change for $p > p_c$ —we conclude that, under coherent unitary errors, the code's logical information is predominantly *scrambled* rather than being erased. In subsequent sections, we will show that random stabilizer codes display a similar phenomenon, underscoring the universal nature of coherent error phase transitions across different types of random code ensembles.

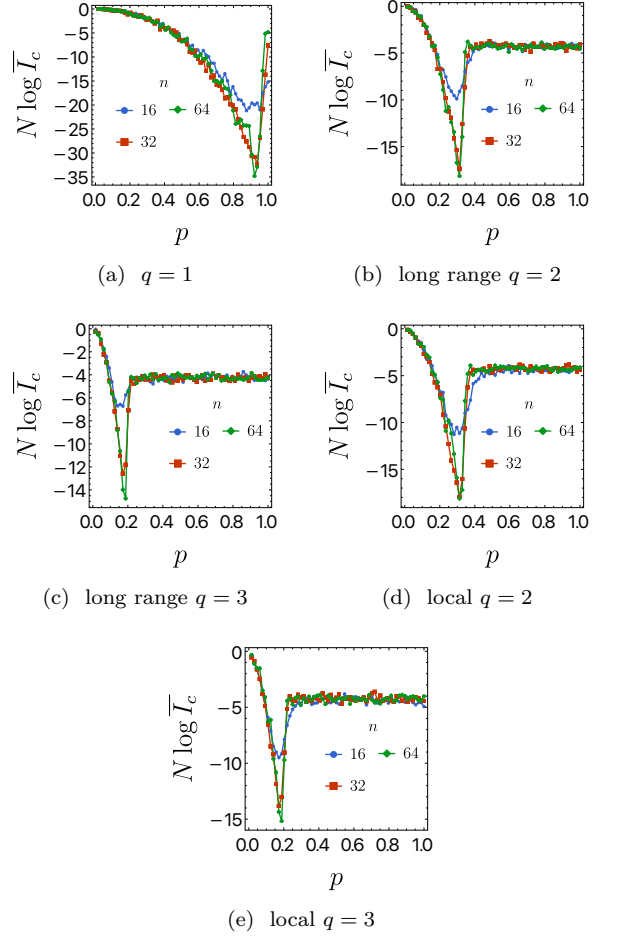


FIG. 9. Coherent information under q -unitary errors for $q = 1, 2, 3$, plotted against the error rate p for various system sizes. Plot (a) shows the single site random unitary model, plots (b)–(c) correspond to the long-range q -unitary model with $q = 1, 2, 3$, while (d)–(e) illustrate the q -local model. Each HGP code is constructed from LDPC $_n(3, 6)$ with $n = 8, 16, 32, 64$.

Syndrome Distribution

The phase transition also manifests in the structure of the syndrome distribution function,

$$\mathbb{P}[s] = \text{Tr}(\Pi_X^{s_X} \Pi_Z^{s_Z} \rho \Pi_Z^{s_Z} \Pi_X^{s_X}). \quad (85)$$

Figure 10 shows the scaling behavior of the *reduced free entropy* φ (as introduced in Eq. 66) for the distribution $\mathbb{P}[s]$. In the large- N limit, φ becomes independent of the system size N , taking the form:

$$\varphi = \begin{cases} F(p) & p < p_c, \\ 0 & p > p_c, \end{cases} \quad (86)$$

where $F(p) > 0$ is a function of the error rate p . Notably, at $p > p_c$, we have $\varphi = 0$, indicating that the distribution

function is essentially uniform:

$$\mathbb{P}[s] = 2^{-N_s}. \quad (87)$$

Under these conditions, any error-correction technique relying on the syndrome distribution fails, and thus p_c here serves as an effective error threshold.

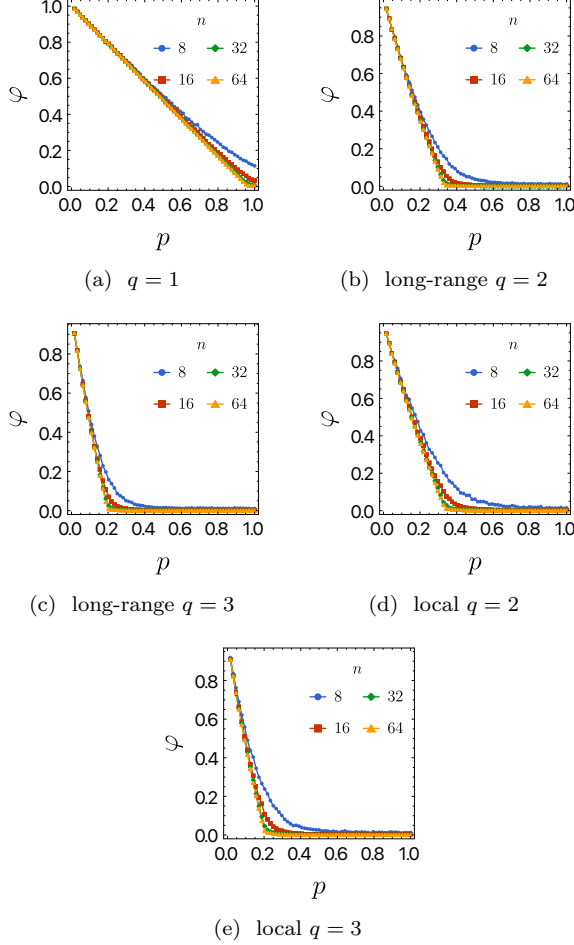


FIG. 10. Scaling of the reduced free entropy density ϕ versus the error probability p for different system sizes $n = 8, 16, 32, 64$. Plot (a) depicts the $q = 1$ single-qubit rotation model; (b) and (c) correspond to the long-range q -unitary model with $q = 2, 3$, while (d) and (e) illustrate the q -local model. Each HGP code is constructed from $\text{LDPC}_n(3, 6)$ with $n = 8, 16, 32, 64$.

Our numerical results suggest that the quantum coherent error phase transition in the HGP code exhibits behavior distinct from that observed in the toric code. Specifically, while the toric code has a finite probability of losing logical information when the error rate exceeds the critical value $p > p_c$, the HGP code instead *scrambles* the logical degrees of freedom within the code space. This scrambling behavior is reminiscent of information scrambling in random quantum circuits. In order to explore this phenomenon more broadly within the random stabilizer code ensemble, we next turn to random codes generated by

random Clifford brickwork circuits, where we find similar signatures of a coherent error induced *scrambling* phase transition.

C. Random Clifford Code

In this section, we introduce another simple model for the RSCE: the *random Clifford code* (RCC)[9–12]. Concretely, we consider an N -qubit quantum code generated by a two-qubit random Clifford brickwork circuit of depth $O(N)$. Of the total N qubits, the first K serve as logical qubits, as illustrated in Fig. 11. We then study the quantum coherent error phase transition under the q -unitary noise model introduced in Sec. IV A.

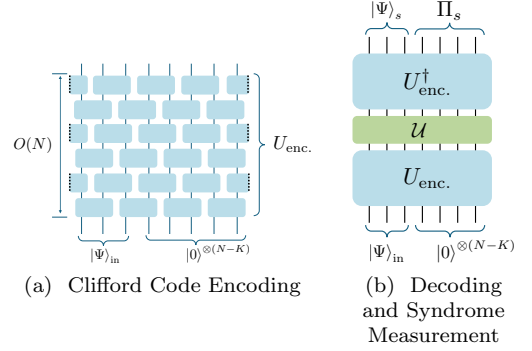


FIG. 11. (a) Encoding by a random Clifford unitary U_{enc} , implemented via a two-qubit random Clifford brickwork circuit of depth $O(N)$. Of the N qubits, the first K store the logical quantum information $|\Psi\rangle_{\text{in}}$, while the remaining qubits function as check qubits. (b) Decoding is performed by the inverse circuit U_{enc}^\dagger , after which a syndrome measurement $\Pi_s = \prod_{i=K+1}^N |s_i\rangle\langle s_i|$ is carried out on the check qubits.

Syndrome Measurement

As with the toric code and HGP code, error correction proceeds by first performing a syndrome measurement and then correcting errors based on the resulting syndrome outcomes $\{s\}$.

For the RCC, the syndrome measurement process is illustrated in Fig. 11b. We apply the decoding unitary $U_{\text{dec}} = U_{\text{enc}}^\dagger$ and then measure all of the $N - K$ “check” qubits. The measurement outcomes, $\{s\}$, serve as the syndromes. The post-measurement (syndrome) state is

$$\begin{aligned} \rho_s &= |\Psi\rangle_s \langle \Psi|_s \\ &= \mathbb{P}[s]^{-1} \Pi_C^s U_{\text{dec}} \rho U_{\text{dec}}^\dagger \Pi_C^s, \end{aligned} \quad (88)$$

where

$$\Pi_C^s = \prod_{i=K+1}^N |s_i\rangle\langle s_i| \quad (89)$$

represents single-qubit projective measurements on the check qubits, conditioned on the syndrome $\{s\}$. Each check qubit is measured in the Z basis, satisfying $Z_i |s_i\rangle = s_i |s_i\rangle$.

In the sections that follow, we examine both the quantum properties of ρ_s and the structure of the syndrome distribution $\mathbb{P}[s]$ to characterize the coherent error phase transition in the RCC.

Syndrome State Logicals

We now examine how coherent errors and syndrome measurements modify the logical information. Consider an initial logical state

$$|\Psi\rangle_{\text{in}} = |0\rangle^{\otimes K}, \quad (90)$$

which is stabilized by the logical stabilizer group

$$G_{\mathcal{L}} = \langle Z_1, Z_2, \dots, Z_K \rangle. \quad (91)$$

To assess the evolution of the logical stabilizers under coherent errors and syndrome measurements, we examine the per-logical-qubit group difference signature

$$\delta_{\text{Logi.}} = \frac{1}{K} \Delta_{\text{Logi.}}^{\mathcal{G}'_{\mathcal{L}}}. \quad (92)$$

where

$$\Delta_{\text{Logi.}}^{\mathcal{G}'_{\mathcal{L}}} = \log_2 |G_{\text{comb.}}| - \log_2 |G_{\mathcal{L}}| \quad (93)$$

is the group difference signature, and the combined group is

$$G_{\text{comb.}} = \langle G_{\mathcal{L}}, G_{\mathcal{L}}', G_{i=K+1, \dots, N} \rangle / \langle G_{i=K+1, \dots, N} \rangle, \quad (94)$$

Here $G'_{\mathcal{L}}$ denotes the set of emergent logical stabilizers in the post-measurement state ρ_s , $G_{\mathcal{L}}$ is the original logical stabilizer group, and

$$G_{i=K+1, \dots, N} = U_{\text{enc.}} Z_{i=K+1, \dots, N} U_{\text{enc.}}^\dagger. \quad (95)$$

are the quantum code checks of RCC.

Similar to that in the HGP code case, we observe a phase transition in $\delta_{\text{Logi.}}$ as we tune the error probability p , for both q -local and long-range q -unitary models. Specifically, for $q > 1$,

$$\delta_{\text{Logi.}} = \begin{cases} 0, & p < p_c, \\ 1, & p > p_c, \end{cases} \quad (96)$$

while for $q = 1$, we find $\delta_{\text{Logi.}} = 0$ for $p < p_c$ and $\delta_{\text{Logi.}} > 0$ when $p > p_c$. Once p exceeds p_c , the logical operators are substantially altered, indicating that the encoded logical information cannot be recovered through a straightforward decoding approach.

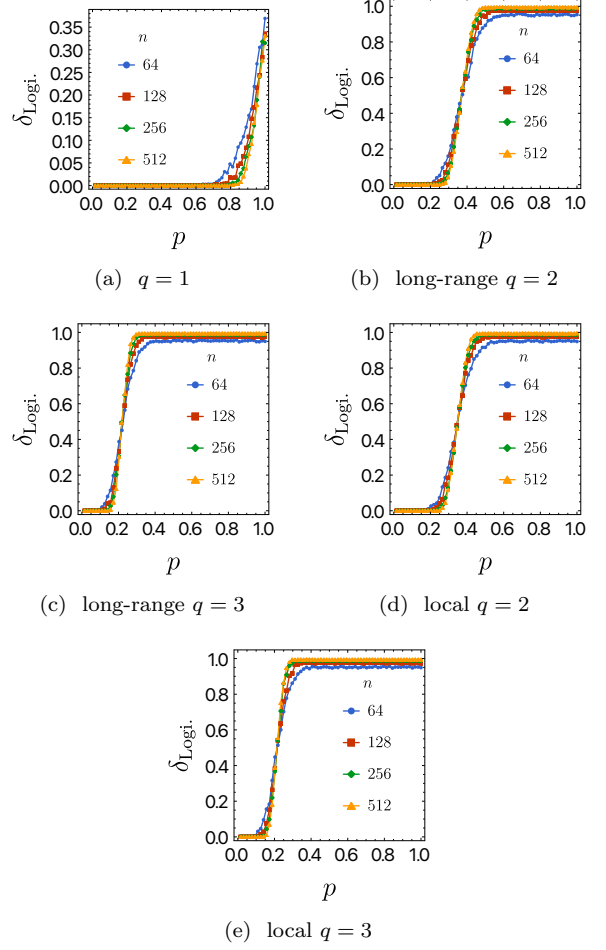


FIG. 12. The density of changes in the logical operators, $\delta_{\text{Logi.}}$, plotted against the error rate p for various system sizes $N = 64, 128, 256, 512$. The parameter q denotes the q -unitary interactions. Plots (a) show $q = 1$; (b) and (c) correspond to the long-range q -unitary model with $q = 2, 3$; (d) and (e) illustrate the q -local model with $q = 2, 3$. Each RCC has a finite code rate, with $K = \frac{1}{4}N$ logical qubits.

Coherent Information

To further characterize the behavior of the logical information under coherent errors, we introduce K reference qubits, each forming a Bell pair with one of the K input logical qubits. Concretely, consider:

$$|\Psi\rangle_{RC} = \frac{1}{2^{K/2}} \bigotimes_{i=1}^K (|0\rangle_i |0\rangle_i^r + |1\rangle_i |1\rangle_i^r), \quad (97)$$

where $|\dots\rangle_i$ labels the i -th logical qubit and $|\dots\rangle_i^r$ labels the corresponding reference qubit. The *coherent information* between the code qubits and reference qubits is then encoded in their entanglement.

Similar to the HGP code, we focus on a *per-logical*-

qubit measure of coherent information:

$$\bar{I}_c = -\frac{1}{K} I(\rho_Q, \mathcal{E}_e), \quad (98)$$

where $I(\rho_Q, \mathcal{E}_e)$ (defined in Eq. 34) is the total coherent information, K is the total number of logical qubits, and $\rho_Q = |\Psi\rangle_{RC} \langle \Psi|_{RC}$.

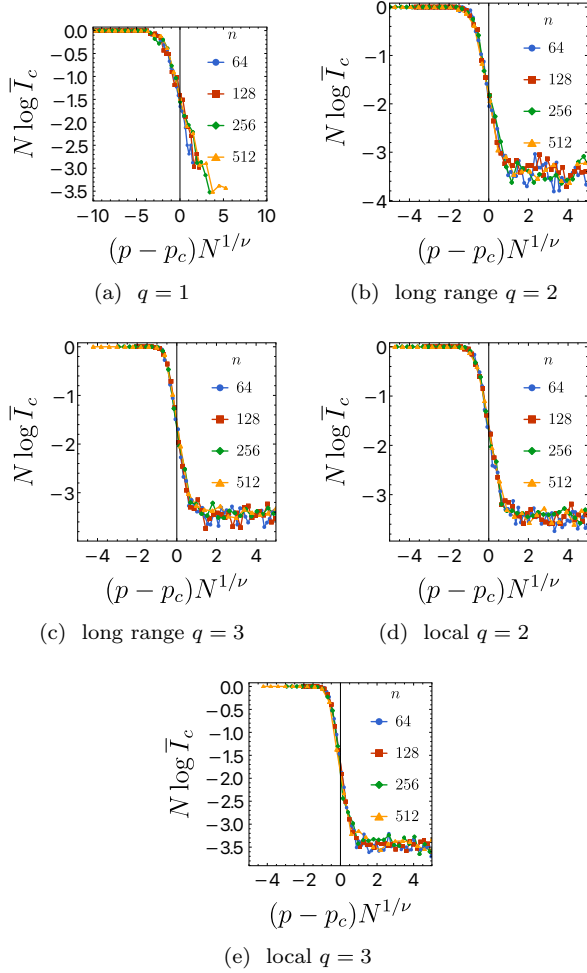


FIG. 13. Coherent information under q -unitary errors for $q = 1, 2, 3$. (a) corresponds to the single-site random unitary model (with $p_c \approx 0.89, \nu \approx 1.61$), (b) and (c) show the long-range q -unitary model (with $q = 2, 3$ and $p_c \approx 0.31, 0.18, \nu \approx 1.92$), whereas (d) and (e) illustrate the q -local model ($p_c \approx 0.29, 0.18, \nu \approx 1.92$).

Figure 13 reveals that for $p < p_c$, the per-qubit coherent information remains close to 1, indicating preserved logical information. Conversely, for $p > p_c$, partial information loss occurs, manifested by $\bar{I}_c < 1$. A more precise characterization shows:

$$\bar{I}_c = \begin{cases} 1, & p < p_c, \\ \exp(-\frac{A}{N}), & p > p_c, \end{cases} \quad (99)$$

where $A > 0$ is an $O(1)$ constant. We further observe a robust data collapse when plotting

$$\log \bar{I}_c = N^{-1} f((p - p_c) L^{1/\nu}), \quad (100)$$

for some scaling function f , and $\nu = 1.61$ for $q = 1$, $\nu = 1.92$ for $q > 1$.

Syndrome Distribution

We now investigate the structure of the syndrome distribution function $\mathbb{P}[s]$. As in the HGP code case, we examine the *reduced free entropy* φ , defined in Eq. 66.

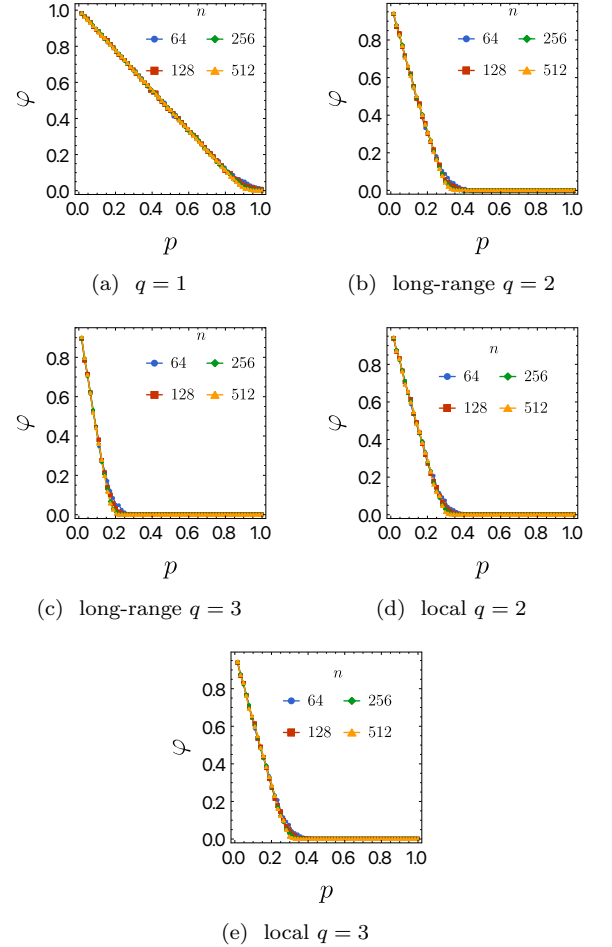


FIG. 14. Scaling of the reduced free entropy density φ as a function of the error probability p for various system sizes $N = 64, 128, 256, 512$. Plot (a) depicts the $q = 1$ single-qubit rotation model; (b) and (c) correspond to the long-range q -unitary model with $q = 2, 3$, while (d) and (e) illustrate the q -local model with $q = 2, 3$.

As shown in Fig. 14, for large system size N :

$$\varphi = \begin{cases} F(p), & p < p_c, \\ 0, & p > p_c, \end{cases} \quad (101)$$

where $F(p) > 0$ is a function of the error rate p . Once p exceeds p_c , we find $\varphi = 0$, indicating that the distribution becomes essentially uniform:

$$\mathbb{P}[s] = 2^{-N_s}. \quad (102)$$

Under these conditions, any error-correction method relying on the syndrome distribution fails, so p_c serves as an effective threshold for coherent errors.

These findings suggest that for $p < p_c$, error correction remains feasible, permitting recovery of the input state $|\Psi\rangle_{\text{in}}$. However, beyond the threshold ($p > p_c$), the coherent information saturates as $\bar{I}_c \sim \exp(-1/N)$. While the logical information may persist in the large- N limit, the uniform nature of the syndrome distribution at $p > p_c$ prevents any syndrome-based decoding protocol from restoring it. Consequently, p_c marks the regime in which coherent errors render the system's logical degrees of freedom essentially unrecoverable.

V. CONCLUSION AND DISCUSSION

In this work, we have demonstrated that coherent unitary errors can induce a *phase transition* in certain quantum stabilizer codes in the thermodynamic limit. By focusing on logical information encoded in the physical qubits, we identified a critical error threshold p_c . Above p_c , syndrome measurements project the logical state onto a different logical state, effectively corrupting the encoded information. Below p_c , the logical state remains the same (up to some single qubit Pauli rotation), allowing for successful recovery through appropriate error-correction procedures.

We illustrated these findings using two representative classes of quantum error-correcting code (QECC) models. First, we applied our framework to the toric code [4, 6], introducing coherent errors on plaquettes via random Clifford unitaries. Numerically, we showed that the logical information (as indicated by the coherent information shared with reference qubits) remains invariant below a critical error density p_c . Above p_c , however, this information can become irrecoverable with finite probability, marking a phase transition in the code's error-correcting capacity.

Second, we examined random stabilizer code ensembles, including the qLDPC (HGP) code [7, 8] and random Clifford code [9–12]. In these models, coherent errors are implemented through either *long-range* q -unitary gates or *q-local* unitaries, reflecting diverse possibilities for multi-qubit interactions. Below p_c , the syndrome state and logical stabilizers remain sufficiently the same as the original ones, up to single qubit Pauli rotation. Above p_c , the logical stabilizers are altered. Further analysis of the coherent information reveals that while the logical information persists in the large N limit, it becomes effectively scrambled, preventing successful syndrome-based decoding.

Our results confirm that coherent errors pose unique challenges for quantum error correction. While bit-flip or phase-flip errors merely change the sign of the logical stabilizers, the nontrivial action of local coherent unitaries can alter the logical stabilizers themselves during the error-correction process. In codes with locality (e.g., the toric code), this transition manifests in both global and local structure of the syndrome state and syndrome distribution function. For random codes lacking a strict notion of locality, analogous transitions appear in the global structure of the syndrome state's quantum properties and in the classical aspects of its syndrome distribution function. At the critical threshold p_c , these measures reveal a change from short- to long-range correlations or show derivative discontinuities, mirroring conventional phase transitions in statistical mechanics.

Overall, our observations underscore that coherent unitary errors can drive a fundamental transition in the behavior of quantum error-correcting codes. By identifying the critical threshold p_c and characterizing the structure of the syndrome distribution above and below it, we make progress toward bridging the gap between quantum error correction, statistical mechanics, and computational complexity theory. We hope that this work inspires further investigation into robust decoding strategies and code constructions designed to mitigate coherent errors in practical quantum technologies.

Several interesting questions remain open. One is the development of decoders specifically tailored to coherent errors, which will likely require more advanced techniques than those used for incoherent noise. Another intriguing direction is that coherent errors can induce effective unitary rotations within the logical subspace. This insight suggests a potentially simple and experimentally accessible method for generating logical gates in surface codes and random codes: applying controlled local unitary rotations on physical qubits followed by syndrome measurements. We expect that such operations will be robust against noise, as this protocol is inherently protected by the QECC. We leave them for future investigation.

ACKNOWLEDGMENTS

We gratefully acknowledge the computing resources provided by Research Services at Boston College and the invaluable assistance of Wei Qiu. We are grateful to Yaodong Li, Shengqi Sang, Tianci Zhou and Timothy Hsieh for their insightful discussions. This research was supported in part by the National Science Foundation under Grant No. DMR-2219735.

Appendix A: Pauli Sampling on Quantum Stabilizer States

In this section, we describe how to compute the probability distribution function for syndrome outcomes result-

ing from Pauli-type measurements on a stabilizer state. Consider a commuting set of M Pauli observables,

$$\mathcal{O} = \{O_1, \dots, O_M\}, \quad (\text{A1})$$

which serve as our measurement operators. Measuring these observables projects the state onto their joint eigenspace, with measurement outcomes labeled by $s = \{s_i = \pm 1\}$.

Let the pre-measurement stabilizer group be

$$G = \langle g_1, \dots, g_N \rangle \quad (\text{A2})$$

for a N -qubit quantum state ρ_G . After the measurement, the post-measurement stabilizer group for the quantum state ρ_{G_s} becomes

$$G_s = \langle s_i O_i, \lambda_l g'_l \rangle, \quad (\text{A3})$$

where the $g'_l = \prod_{j=1}^N g_j^{R_{j,l}}$'s are group elements inherent from the pre-measurement group G with $R_{j,l} = 0, 1$ and $\lambda_l = \pm 1$ are their corresponding eigenvalues (or charges) with respect to the state $g'_l \rho_G = \lambda_l \rho_G$.

Measurement outcome distribution

Not all measurement outcomes are independent; they must satisfy certain constraints inherited from the original stabilizers. In particular, for each stabilizer $g_l \in G$ that is compatible with the measurement, there exists a binary vector Q_l (with components $Q_{i,l} \in \{0, 1\}$) such that

$$g_l \propto \prod_{i=1}^M O_i^{Q_{i,l}}, \quad (\text{A4})$$

and the measurement outcomes must satisfy

$$\lambda_l \prod_{i=1}^M (s_i)^{Q_{i,l}} = q_l \quad \forall l, \quad (\text{A5})$$

with $q_l = \text{sign Tr}(g_l \prod_{i=1}^M O_i^{Q_{i,k}})$ and λ_l being the charge of stabilizer $g_l \in G$.

The binary coefficients $Q_{i,l}$ can be determined by examining the null space of the commutator matrix T , defined by

$$T_{i,j} = \begin{cases} 0 & \text{if } [O_i, g_j] = 0, \\ 1 & \text{if } [O_i, g_j] \neq 0. \end{cases} \quad (\text{A6})$$

Solving

$$\sum_{i=1}^M Q_{i,l} T_{i,j} \equiv 0 \pmod{2} \quad \forall j, l \quad (\text{A7})$$

identifies the null vectors over \mathbb{F}_2 and thus yields the coefficients $Q_{i,l}$.

In stabilizer systems, measurements of observables that are not part of the stabilizer group yield equiprobable outcomes. In contrast, measurements of compatible observables directly reveal the charge of certain stabilizer, thereby imposing constraints on the measurement results. Consequently, the syndrome outcome distribution can be written as

$$\mathbb{P}[s] = Z^{-1} \prod_{k=1}^{r_Q} \delta_k[s], \quad (\text{A8})$$

with

$$\delta_k[s] = \frac{1}{2} \left(1 + \lambda_k \prod_{i=1}^{N_s} (s_i)^{Q_{i,k}} \right), \quad (\text{A9})$$

where N_s is the total number of measurements and r_Q is the number of linearly independent constraints (i.e. the number of independent binary vectors Q_k). The normalization factor Z is the partition function given by

$$Z = \sum_s \prod_{k=1}^{r_Q} \delta_k[s] = 2^{M-r_Q}. \quad (\text{A10})$$

Post-measurement Stabilizer Structure

After measuring the M observables, the post-measurement stabilizer group G' remains abelian, so each generator g'_l can be written as

$$g'_l = \prod_{j=1}^N g_j^{R_{j,l}}, \quad (\text{A11})$$

where the binary coefficients $R_{j,l} \in \{0, 1\}$ satisfy the commutativity constraints

$$\sum_{j=1}^N T_{i,j} R_{j,l} \equiv 0 \pmod{2} \quad \forall i, l. \quad (\text{A12})$$

Here $T_{i,j}$ is the commutator matrix from Eq. A6. Since there are N original generators and $\text{rank}(T)$ independent constraints, the number of independent post-measurement stabilizers is

$$n_g = N - \text{rank}(T). \quad (\text{A13})$$

In addition to these “determined” stabilizers, there are $n_o = \text{rank}(T)$ *free observables* whose measurement outcomes $s_k = \pm 1$ are random. We label them

$$O'_k = \prod_{i=1}^M O_i^{\tilde{Q}_{i,k}}, \quad \tilde{Q} = Z_2^M \setminus Q, \quad (\text{A14})$$

where $Q \subset Z_2^M$ is the solution space of $TQ = 0$. Thus the full post-measurement stabilizer group is

$$G_s = \langle s_k O'_k, \lambda_l g'_l \rangle, \quad (\text{A15})$$

and its total rank is

$$\text{rank}(G_s) = n_g + n_o = N,$$

so A15 indeed provides a complete generating set.

Finally, if we average (trace out) over all free-observable outcomes, we recover the mixed state

$$\bar{\rho}_{G'} = \sum_s \Pi_s \rho_G \Pi_s,$$

whose stabilizer subgroup is

$$\overline{G_s} = \langle g'_l = \prod_{j=1}^N g_j^{R_{j,l}} \mid l = 1, \dots, N - \text{rank}(T) \rangle.$$

-
- [1] J. Preskill, Quantum computing in the nisq era and beyond, *Quantum* **2**, 79 (2018).
- [2] M. A. Nielsen and I. L. Chuang, *Quantum computation and quantum information* (Cambridge university press, 2010).
- [3] D. Aharonov and M. Ben-Or, Fault-tolerant quantum computation with constant error, in *Proceedings of the twenty-ninth annual ACM symposium on Theory of computing* (1997) pp. 176–188.
- [4] A. Y. Kitaev, Fault-tolerant quantum computation by anyons, *Annals of physics* **303**, 2 (2003).
- [5] A. G. Fowler, M. Mariantoni, J. M. Martinis, and A. N. Cleland, Surface codes: Towards practical large-scale quantum computation, *Physical Review A—Atomic, Molecular, and Optical Physics* **86**, 032324 (2012).
- [6] E. Dennis, A. Kitaev, A. Landahl, and J. Preskill, Topological quantum memory, *Journal of Mathematical Physics* **43**, 4452 (2002).
- [7] J.-P. Tillich and G. Zémor, Quantum ldpc codes with positive rate and minimum distance proportional to the square root of the blocklength, *IEEE Transactions on Information Theory* **60**, 1193 (2013).
- [8] A. Leverrier, J.-P. Tillich, and G. Zémor, Quantum expander codes, in *2015 IEEE 56th Annual Symposium on Foundations of Computer Science (IEEE, 2015)* pp. 810–824.
- [9] W. Brown and O. Fawzi, Short random circuits define good quantum error correcting codes, in *2013 IEEE International Symposium on Information Theory (IEEE, 2013)* pp. 346–350.
- [10] J. Nelson, G. Bentsen, S. T. Flammia, and M. J. Gullans, Fault-tolerant quantum memory using low-depth random circuit codes, *arXiv preprint arXiv:2311.17985* (2023).
- [11] A. S. Darmawan, Y. Nakata, S. Tamiya, and H. Yamasaki, Low-depth random clifford circuits for quantum coding against pauli noise using a tensor-network decoder, *Phys. Rev. Res.* **6**, 023055 (2024).
- [12] M. J. Gullans, S. Krastanov, D. A. Huse, L. Jiang, and S. T. Flammia, Quantum coding with low-depth random circuits, *Phys. Rev. X* **11**, 031066 (2021).
- [13] E. Knill, R. Laflamme, and W. H. Zurek, Resilient quantum computation: error models and thresholds, *Proceedings of the Royal Society of London. Series A: Mathematical, Physical and Engineering Sciences* **454**, 365 (1998).
- [14] C. T. Chubb and S. T. Flammia, Statistical mechanical models for quantum codes with correlated noise, *Annales de l’Institut Henri Poincaré D* **8**, 269 (2021).
- [15] B. M. Terhal, Quantum error correction for quantum memories, *Rev. Mod. Phys.* **87**, 307 (2015).
- [16] H. Bombin, R. S. Andrist, M. Ohzeki, H. G. Katzgraber, and M. A. Martin-Delgado, Strong resilience of topological codes to depolarization, *Phys. Rev. X* **2**, 021004 (2012).
- [17] S. Bravyi, M. Englbrecht, R. König, and N. Peard, Correcting coherent errors with surface codes, *npj Quantum Information* **4**, 55 (2018).
- [18] E. H. Chen, G.-Y. Zhu, R. Verresen, A. Seif, E. Bäumer, D. Layden, N. Tantivasadakarn, G. Zhu, S. Sheldon, A. Vishwanath, *et al.*, Nishimori transition across the error threshold for constant-depth quantum circuits, *Nature Physics*, 1 (2024).
- [19] G.-Y. Zhu, N. Tantivasadakarn, A. Vishwanath, S. Trebst, and R. Verresen, Nishimori’s cat: Stable long-range entanglement from finite-depth unitaries and weak measurements, *Phys. Rev. Lett.* **131**, 200201 (2023).
- [20] J. Behrends and B. Béri, The surface code under generic x -error channels: Statistical mechanics, error thresholds, and errorfield double phenomenology, *arXiv preprint arXiv:2412.21055* (2024).
- [21] Á. Márton and J. K. Asbóth, Coherent errors and readout errors in the surface code, *Quantum* **7**, 1116 (2023).
- [22] F. Venn, J. Behrends, and B. Béri, Coherent-error threshold for surface codes from majorana delocalization, *Phys. Rev. Lett.* **131**, 060603 (2023).
- [23] J. Behrends, F. Venn, and B. Béri, Surface codes, quantum circuits, and entanglement phases, *Phys. Rev. Res.* **6**, 013137 (2024).
- [24] Y. Bao and S. Anand, Phases of decodability in the surface code with unitary errors, *arXiv preprint arXiv:2411.05785* (2024).
- [25] Z. Cheng, E. Huang, V. Khemani, M. J. Gullans, and M. Ippoliti, Emergent unitary designs for encoded qubits from coherent errors and syndrome measurements, *arXiv preprint arXiv:2412.04414* (2024).
- [26] B. Skinner, J. Ruhman, and A. Nahum, Measurement-induced phase transitions in the dynamics of entanglement, *Physical Review X* **9**, 031009 (2019).
- [27] M. J. Gullans and D. A. Huse, Dynamical purification phase transition induced by quantum measurements, *Physical Review X* **10**, 041020 (2020).
- [28] Y. Li, X. Chen, and M. P. Fisher, Measurement-driven entanglement transition in hybrid quantum circuits, *Physical Review B* **100**, 134306 (2019).
- [29] Y. Li, X. Chen, and M. P. Fisher, Quantum zeno effect and the many-body entanglement transition, *Physical Review B* **98**, 205136 (2018).
- [30] M. P. A. Fisher, V. Khemani, A. Nahum, and S. Vijay, Random Quantum Circuits, *Ann. Rev. Condensed Matter Phys.* **14**, 335 (2023), *arXiv:2207.14280 [quant-ph]*.
- [31] Y. Zhao and D. E. Liu, An analytic study of the independent coherent errors in the surface code, *arXiv preprint arXiv:2112.00473* (2021).

- [32] H. Bombin and M. A. Martin-Delgado, Statistical mechanical models and topological color codes, *Phys. Rev. A* **77**, 042322 (2008).
- [33] S. Bravyi and R. Raussendorf, Measurement-based quantum computation with the toric code states, *Phys. Rev. A* **76**, 022304 (2007).
- [34] H. Liu, V. Ravindranath, and X. Chen, Quantum entanglement phase transitions and computational complexity: Insights from ising models, *arXiv preprint arXiv:2310.01699* (2023).
- [35] R. Koenig and J. A. Smolin, How to efficiently select an arbitrary clifford group element, *Journal of Mathematical Physics* **55** (2014).
- [36] B. Schumacher and M. A. Nielsen, Quantum data processing and error correction, *Phys. Rev. A* **54**, 2629 (1996).
- [37] S. Lloyd, Capacity of the noisy quantum channel, *Phys. Rev. A* **55**, 1613 (1997).
- [38] L. Colmenarez, Z.-M. Huang, S. Diehl, and M. Müller, Accurate optimal quantum error correction thresholds from coherent information, *Physical Review Research* **6**, L042014 (2024).
- [39] S. Sang and T. H. Hsieh, Stability of mixed-state quantum phases via finite markov length, *arXiv preprint arXiv:2404.07251* (2024).
- [40] F. G. S. L. Brandão, A. W. Harrow, J. Oppenheim, and S. Strelchuk, Quantum conditional mutual information, reconstructed states, and state redistribution, *Phys. Rev. Lett.* **115**, 050501 (2015).
- [41] O. Fawzi and R. Renner, Quantum conditional mutual information and approximate markov chains, *Communications in Mathematical Physics* **340**, 575 (2015).
- [42] B. Min, Y. Zhang, Y. Guo, D. Segal, and Y. Ashida, Mixed-state phase transitions in spin-holstein models, *Phys. Rev. B* **111**, 115123 (2025).
- [43] Y. Zhang and S. Gopalakrishnan, Conditional mutual information and information-theoretic phases of decohered gibbs states, *arXiv preprint arXiv:2502.13210* (2025).
- [44] H. Liu and X. Chen, Plaquette models, cellular automata, and measurement-induced criticality, *Journal of Physics A: Mathematical and Theoretical* **57**, 435003 (2024).
- [45] A. D. Wyner, A definition of conditional mutual information for arbitrary ensembles, *Information and Control* **38**, 51 (1978).
- [46] D. J. MacKay and R. M. Neal, Near shannon limit performance of low density parity check codes, *Electronics letters* **33**, 457 (1997).
- [47] M. Mezard and A. Montanari, *Information, physics, and computation* (Oxford University Press, 2009).